Earth Planet. Sci. Lett. 667 (2025) 119516

Contents lists available at ScienceDirect

Earth and Planetary Science Letters

journal homepage: www.elsevier.com/locate/epsl

Petrogenesis of cogenetic silica-undersaturated and -oversaturated rocks: Quantifying the role of crustal assimilation

Caroline R. Soderman [a,*], Owen M. Weller [a], Alex Copley [a], Adrian A. Finch [b], Charles D. Beard [c]

[a] Dept. of Earth Sciences, University of Cambridge, CB2 3EQ, UK
[b] School of Earth and Environmental Sciences, University of St Andrews, KY16 9TS, UK
[c] Dept. of Earth Sciences, Utrecht University, 3584 CB Utrecht, the Netherlands

ARTICLE INFO

Editor: R. Hickey-Vargas

ABSTRACT

Crustal assimilation during fractional crystallisation is commonly proposed as a mechanism to generate evolved silica-oversaturated (i.e. quartz normative) rocks alongside cogenetic silica-undersaturated (i.e. feldspathoid normative) rocks. However, the amount of required assimilation, and the impact of varying crystallisation parameters (e.g. pressure, oxygen fugacity), remain poorly understood, despite a petrogenetic framework for these cogenetic rocks being necessary for understanding their varied magmatic critical metal enrichment. Here we apply new thermodynamic models to a case study of the Younger Giant Dyke Complex in south Greenland, a layered intrusive complex with cogenetic evolved silica-undersaturated and -oversaturated rocks, to explore quantitatively the role of these processes during fractionation and assimilation. A range of assimilation scenarios is explored, alongside thermal and isotopic perspectives on these scenarios. Our calculations show that a phase equilibria approach can tightly constrain assimilant amounts (e.g. 0–≤ 15% assimilation by mass of country rock granite in this complex), because of the narrow compositional range that divides silica-undersaturated from silica-oversaturated melts, whereas thermal and isotopic approaches may permit wider ranges of assimilation estimates because their model input parameters tend to be more variable. In general, silica-undersaturated primitive melts crystallising at more reduced conditions and/or higher pressures require more crustal assimilation to become silica-oversaturated. Consequently, the formation of evolved silica-undersaturated rocks is favoured when fractionation occurs at lower oxygen fugacity and higher pressures, because magmas are more protected from the effects of assimilation. Understanding such behaviour may be an important part of decoding why some alkaline-silicate complexes develop high concentrations of critical metals.

1. Introduction

The origin of cogenetic evolved silica-undersaturated and -oversaturated igneous rocks is an ongoing petrological problem because the two regimes are separated by thermal divides in both primitive and evolved systems (e.g. in the canonical clinopyroxene–nepheline–olivine–quartz ‘basalt tetrahedron’ and the quartz-nepheline-kalsilite system; Bowen, 1937; Tuttle and Bowen, 1958; Yoder Jr. and Tilley, 1962). Nevertheless, numerous alkaline-silicate complexes around the world show cogenetic examples of both rock types (e.g. the Canadian Blatchford Lake and Mount Brome complexes, the Greenlandic Ilimmaasaq – previously spelled Ilímaussaq – and Kangerlussuaq complexes, and the Norwegian Larvik complex; Neumann, 1980; Chen et al., 1994; Riishuus et al., 2006; Upton, 2013; Marks and Markl, 2015). Constraining the controls on the formation of these alkaline-silicate complexes, and their relative state of silica saturation, is important because some host large deposits of critical metals (e.g. rare earth elements), with the deposit type, size, mineralogy, and exploration indicators being intimately linked to the silica content of their melts (Beard et al., 2023).

Several processes have been invoked to explain the compositional diversity in such complexes. Where the primitive melts are silica-saturated, magma recharge by alkali-rich melts (e.g. Möller and Williams-Jones, 2016) or variable fractionation pressures (with lower pressure fractionation producing silica-oversaturated melts and higher pressure fractionation producing silica-undersaturated melts; Neumann, 1980; Rämö et al., 2022; Soderman et al., 2025) can explain the ob-

---

* Corresponding author.
E-mail address: cs801@cam.ac.uk (C.R. Soderman).

https://doi.org/10.1016/j.epsl.2025.119516
Received 19 December 2024; Received in revised form 22 May 2025; Accepted 19 June 2025

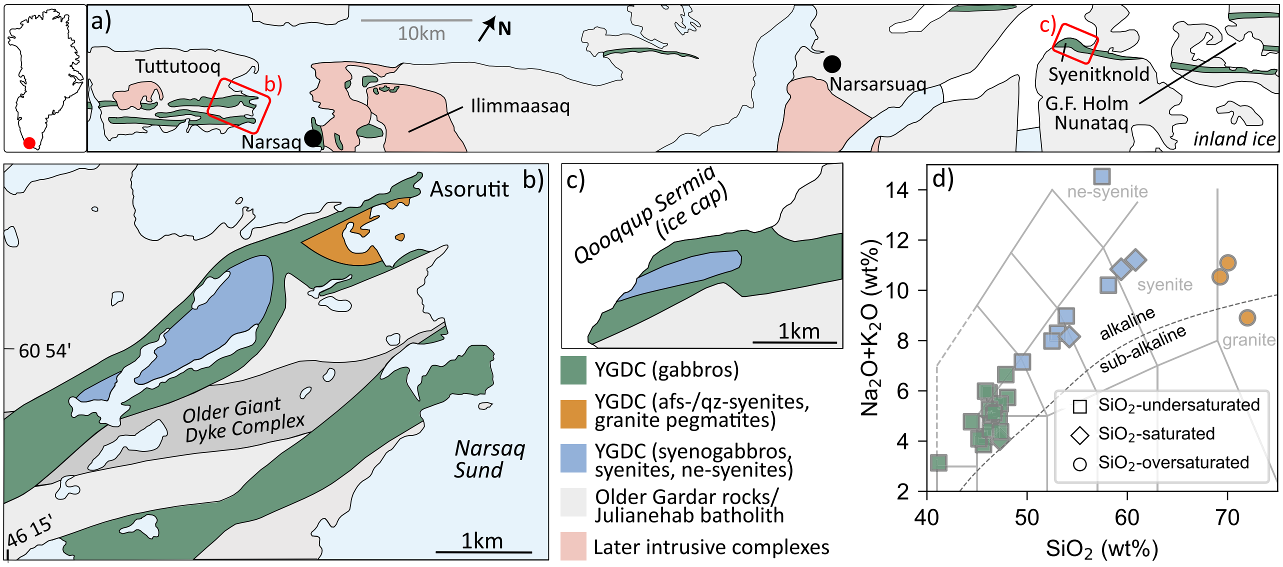

Fig. 1. Geological map of some of the Younger Giant Dyke Complex (YGDC) exposed in south Greenland (continued extensions to SW and NE exist), and reported whole-rock geochemistry. a) and b) modified from Upton (2013); Koopmans et al. (2022); c) modified from Upton and Fitton (1985). d) Published whole-rock YGDC compositions in total alkali-silica (TAS) space classified according to normative mineralogy (see supplement for sample details and normative mineralogy classification).

served compositional diversity. However, where primitive melts are silica-undersaturated, the processes that can generate cogenetic silica-oversaturated melts are limited, with assimilation of silica-rich country rocks being commonly proposed (e.g. Foland et al., 1993; Riishuus et al., 2006). These initially silica-undersaturated systems may be more likely to be enriched in incompatible elements (e.g. rare earth elements) relative to silica-saturated melts, as they likely form from lower degrees of mantle melting, making them of particular interest among alkaline-silicate complexes worldwide for their potential critical metal enrichment (e.g. Ilimmaasaq).

Assimilation is often supported by isotope and trace element data, and the amount of crustal material assimilated can be constrained using mixing models (e.g. Foland et al., 1993; Taylor and Upton, 1993; Chen et al., 1994; Landoll and Foland, 1996; Stevenson et al., 1997; Harris et al., 1999; Riishuus et al., 2006; Roulleau and Stevenson, 2013), commonly invoking simultaneous assimilation-fractional crystallisation (AFC; DePaolo, 1981). However, the range of viable assimilation proportions constrained using such models can be wide or unresolvable, especially in systems where the trace element chemistry of possible assimilants and primitive melts are highly variable, or difficult to determine (Landoll and Foland, 1996; Riishuus et al., 2006). Models that additionally consider major element behaviour and energy balance as assimilation constraints (e.g. Spera and Bohrson, 2001; Bohrson and Spera, 2001; Bohrson et al., 2014, 2020; Heinonen et al., 2020) have not been widely applied in alkaline-silicate complexes. Therefore, in these systems, the amount of crustal assimilation needed to generate observed chemical and isotopic diversity is poorly constrained, limiting our petrogenetic understanding of their varied critical metal enrichment characteristics (Beard et al., 2023).

To constrain the effects of assimilation on a silica-undersaturated primitive melt, we model fractional crystallisation and assimilation using new thermodynamic models for sub-alkaline to alkaline igneous rocks (Weller et al., 2024). We use a case study of the Younger Giant Dyke Complex (YGDC) in south Greenland, an elongate, anastomosing layered intrusion with branches ≤ 800 m wide exposed in several segments along 200 km from Tuttutooq Island (near Narsaq) to G.F. Holm Nunataq, north-east of Narsarsuaq (Fig. 1; Upton, 2013). The YGDC is part of widespread magmatism in south Greenland associated with continental rifting at 1325–1140 Ma (Upton, 2013) and was emplaced into Palaeoproterozoic granitoids (the Julianehåb batholith) at ∼1–2 kbar (Upton and Thomas, 1980; Upton, 1987, 2013). The complex forms an ideal natural laboratory as the silica saturation state of its inner portion varies along strike, evolving from primitive silica-undersaturated compositions in chilled margins to both silica-undersaturated rocks (nepheline-bearing syenites near inland ice at Syenitknold and intermediate syenogabbros on Tuttutooq), and silica-oversaturated rocks (quartz-bearing syenites and granites on Tuttutooq; Upton, 1987); a compositional diversity also seen in the reported whole-rock YGDC chemistry (Fig. 1d). Despite this variability, the reported geochemistry of intrusion margin samples from along the YGDC's length suggests that the complex formed from one large, broadly homogeneous magma batch (Upton et al., 1985; Upton, 2013). Isotope systematics in the wider region suggest that crustal assimilation is involved in the origin of silica-oversaturated rocks. For example, granitic and syenitic intrusions generally have higher $^{87}Sr/^{86}Sr_{initial}$ than more mafic ones (Upton et al., 2003). Intrusions across the rift define Pb isotope mixing trends toward their local host rocks, including at Tuttutooq (Taylor and Upton, 1993; Goodenough, 1997; Upton et al., 2003), but no quantitative estimates of assimilation have been made for the YGDC. AFC calculations using Sr-Nd isotope data suggest that the alkali granite of the Ilimmaasaq central complex formed via 35–40% assimilation (by mass) of the local granitoid crust (Stevenson et al., 1997); the only quantitative estimate of assimilation in the region.

2. Methods

Modelling is performed in MAGEMin (Riel et al., 2022) with thermodynamic database ds6.36 (Holland and Powell, 2011, as modified in Weller et al., 2024). Calculations are performed in the volatile-free Na_2O-CaO-K_2O-FeO-MgO-Al_2O_3-SiO_2-TiO_2-Fe_2O_3 model system. Hydrous phases (e.g. biotite, amphibole) only become a frequent part of the primary assemblage in evolved parts of the YGDC (Upton and Thomas, 1980). Given this distribution, and the absence of a hydrous melt model suitable for alkaline systems, we consider the anhydrous model system appropriate for this study as it focuses on the importance of early crystallisation trajectories for the major element evolution of the melt. Additionally, the effect of small amounts of water (< 1 wt%) on early melt evolution in mafic alkaline systems close to silica-undersaturation (using a related set of composition-dependent equations designed for sub-alkaline systems; Green et al., 2025) has been shown

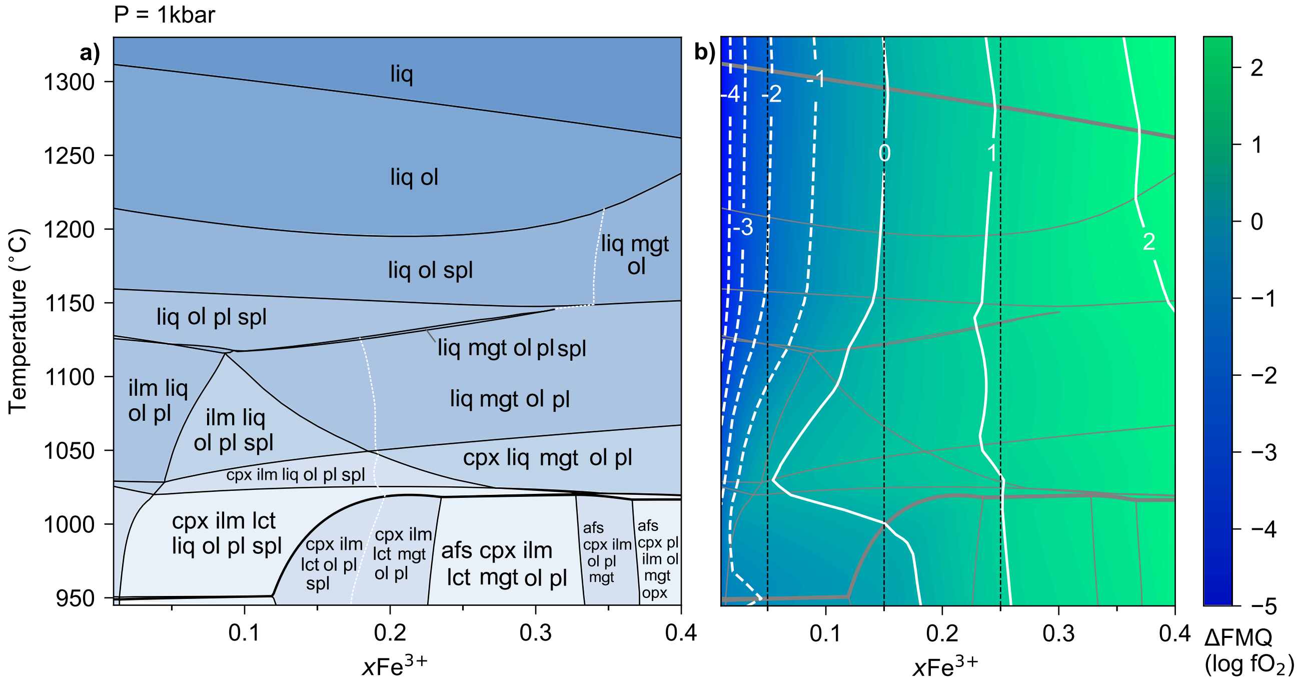

Fig. 2. T-$x\mathrm{Fe}^{3+}$ pseudosection for most primitive chilled YGDC melt composition (Table S2) from $x\mathrm{Fe}^{3+}$ = 0–0.4, where $x\mathrm{Fe}^{3+}$ = molar $\mathrm{Fe}^{3+}/(\mathrm{Fe}^{2+}+\mathrm{Fe}^{3+})$. a) Mineral abbreviations: afs - alkali feldspar, cpx - clinopyroxene, ilm - ilmenite, lct - leucite, ol - olivine, mgt - magnetite, pl - plagioclase, spl - spinel. White dashed line shows supra-solvus transition between spinel and magnetite. b) Pseudosection contoured for ΔFMQ. Bold grey lines show solidus and liquidus. Vertical dashed lines show the three $x\mathrm{Fe}^{3+}$ values used in this study.

to be minor (Soderman et al., 2025). However, as part of a comparison using an alternative modelling approach (the Magma Chamber Simulator (MCS); Bohrson et al., 2014), we also consider the effect of small amounts of water on the evolving melt composition (see Supplement).

We model the compositional evolution of the YGDC using the most MgO-rich (i.e. most primitive) of published chilled margin YGDC samples (a silica-undersaturated basalt from the intrusion margin on Tuttutooq; Upton and Thomas, 1980; Köhler et al., 2009; Table S1). Given the proposed homogeneity of the magma along its length, this composition is considered appropriate for the whole complex. Minor P_2O_5 and MnO are ignored when converting the sample composition to the model system (Table S2). $x\mathrm{Fe}^{3+}$ (molar $\mathrm{Fe}^{3+}/(\mathrm{Fe}^{2+}+\mathrm{Fe}^{3+})$) was not reported, but is explored as a variable (see below) based on oxygen fugacity (fO_2) estimates of primitive YGDC melts of ΔFMQ ∼ −2 to 0 (Upton and Thomas, 1980), where ΔFMQ represents log unit deviations from the fayalite-magnetite-quartz buffer (Fig. 2). Additional model bulk compositions (crustal assimilants, and a more general silica-undersaturated trachybasalt/syenogabbro composition; Cox, 1971) are given in Tables S1–2.

We first model fractional crystallisation of the silica-undersaturated primitive melt (simulated by complete removal of solids every 1 °C of cooling from the liquidus temperature), given the presence of evolved YGDC silica-undersaturated rocks as expected to be formed from a primitive silica-undersaturated melt. Modelling is performed at 1–4 kbar, including the estimates of YGDC crystallisation depth (Upton and Thomas, 1980; Upton, 2013) and extending to higher pressures to allow for investigation of pressure as a variable. Three values of $x\mathrm{Fe}^{3+}$ (0.05, 0.15, 0.25; Table S2) are explored, corresponding to log fO_2 of ΔFMQ ∼ −2, 0 and +1 at the liquidus and solidus of the bulk composition (Fig. 2). These values extend to higher fO_2 than reported for primitive magmas in the region (log fO_2 ΔFMQ ∼ −2 to 0; Upton and Thomas, 1980), permitting investigation of oxidation state as a variable.

Two endmember assimilation and crystallisation scenarios are then considered, given that evolved silica-oversaturated rocks are also observed: AFC (i.e. simultaneous assimilation-fractional crystallisation), and single-stage assimilation followed by subsequent fractional crystallisation. For both scenarios, the assimilant used for modelling is the bulk (i.e. supra-liquidus) composition of the local crust (Julianehåb granitoid, Tables S1–2; Kalsbeek and Taylor, 1985), identified via Pb isotope mixing trends as an assimilant in the YGDC (Taylor and Upton, 1993). An alternative assimilant composition of Archean gneiss from the region (Steenfelt et al., 2005, Tables S1–S2) is also considered for AFC to test the sensitivity of our results to country rock composition.

For the AFC case, modelling starts from the primitive YGDC composition at the liquidus temperature for the calculation pressure. The system is cooled in 1°C steps. The solid material produced is removed from the system at each step to simulate fractional crystallisation. This solid mass is used to calculate the mass of assimilant added into the residual melt prior to the next cooling step (Fig. 3), using a fixed mass ratio of assimilated to fractionated material (A:F ratio, following DePaolo, 1981). The new melt composition for the next cooling step is calculated by adding the required amount of assimilant to the residual melt with simple two-component mixing equations. A:F is fixed during a given assimilation calculation, but is varied between calculations from 0 (pure fractional crystallisation) to 0.3 (reflecting 30% by mass addition of assimilant by the end of fractionation; chosen due to similar estimates of assimilated mass in Ilimmaasaq; Stevenson et al., 1997). These calculations make several implicit assumptions, including that assimilation happens throughout fractionation, that melt is always in contact with country rock, and that no solid-state assimilation occurs after crystallisation of the intrusion.

For single-stage assimilation, a given mass fraction of crustal assimilant (0–0.3, relative to the initial YGDC mass) is added to the primitive YGDC bulk composition with initial $x\mathrm{Fe}^{3+}$ = 0.15, forming an array of compositions extending from the primitive YGDC composition towards the Julianehåb granitoid. These compositions are subsequently fractionally crystallised with 1°C cooling steps at 1 kbar, with no further assimilation. Such a model is appropriate if assimilation happens rapidly relative to fractionation, as implied by some previous studies (e.g. Brandeis and Jaupart, 1987; McLeod and Sparks, 1998), or if assimilation happens immediately following emplacement and subsequently

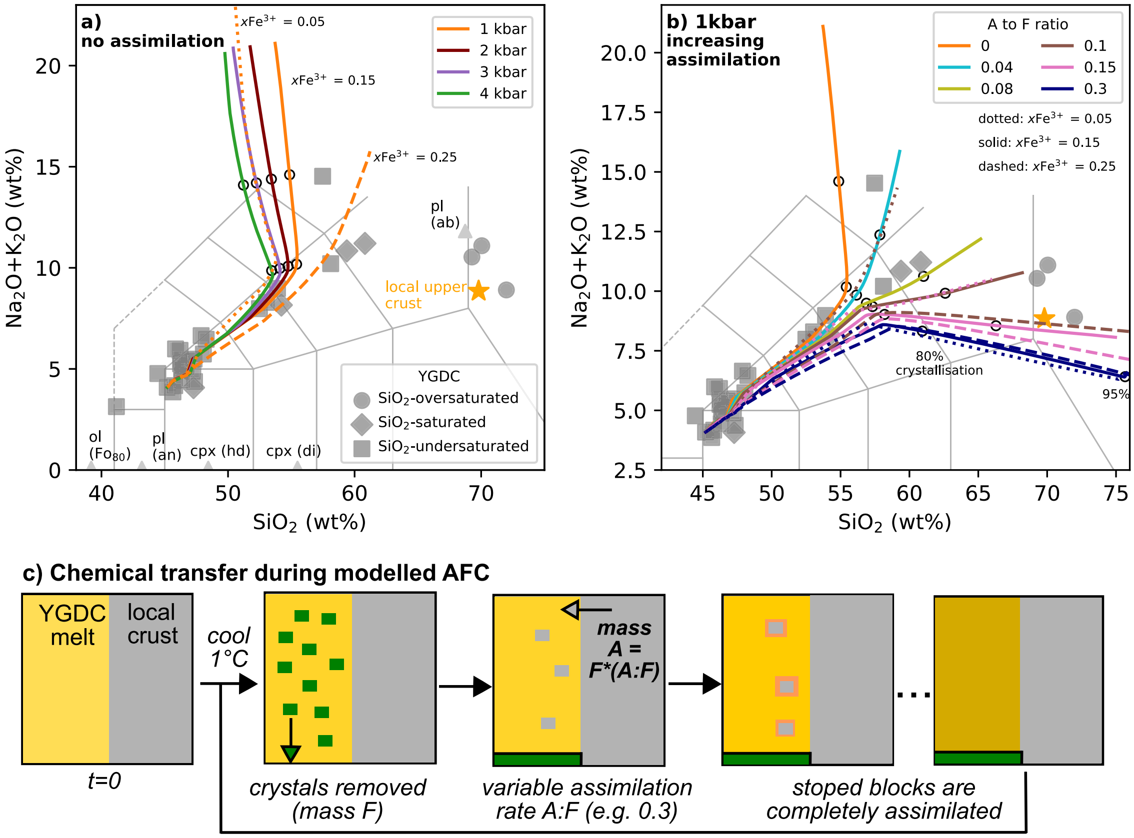

Fig. 3. Melt evolution in total-alkali versus silica (TAS) space during fractional crystallisation and simultaneous assimilation-fractional crystallisation (AFC). (a) Melt evolution during fractional crystallisation of primitive YGDC melt at varying pressure (with $xFe^{3+} = 0.15$) and xFe^{3+} (at 1 kbar). Open circles show 80 and 95 wt% crystallisation for $xFe^{3+} = 0.15$ scenarios. Dark grey symbols show reported compositions of YGDC rocks (as per Fig. 1d), and symbol shape designates normative mineralogy classification (see supplement). Pale grey triangles show SiO$_2$ and Na$_2$O + K$_2$O of example crystallising phases, for reference (ab = albite, an = anorthite, di = diopside, hd = hedenbergite). (b) Melt evolution during assimilation-fractional crystallisation (AFC) of primitive YGDC melt at 1 kbar, with varying assimilation to fractionation ratios (A:F) and xFe^{3+}. Assimilant (star) is Julianehåb granite (Kalsbeek and Taylor, 1985). All fractionation and AFC paths in both panels shown to 98 wt% crystallisation. For reference, the orange solid line is common to both parts of the figure. c) Schematic of the AFC calculation.

ceases due to crystallisation on the intrusion margins preventing further interaction between the melt and country rock.

In both assimilation scenarios, a temperature-independent assimilant composition—the bulk crust—means that we are considering assimilation via stoping, where wallrock blocks are incorporated wholesale into the residual melt (Fig. 3; Bohrson et al., 2020; Heinonen et al., 2021a). This process represents an endmember scenario, without considering assimilation of partial melts of the country rock. For the major and minor elements used as the focus of this study (not trace elements or their isotopes), reported comparisons of assimilation via stoping versus assimilation of wallrock partial melts generally show similar melt chemistry evolution, with only small differences ($\lesssim$ 2 wt%) in any given oxide composition between the two scenarios (Bohrson et al., 2020). This similarity occurs because a low degree partial melt of granite has a relatively similar major element composition to the bulk granite compared to its trace element composition. Therefore, our simplified approach of assimilation by stoping will capture the most important aspects of the major element (and mineral assemblage) evolution of the system for the problem we are trying to address. As a comparison, however, we model additional scenarios (see Supplement) where the assimilant is a partial crustal melt and where assimilation only begins part-way through crystallisation, replicating assimilation via wallrock melting (Bohrson et al., 2020; Heinonen et al., 2021a). In this study, we have also chosen to decouple the phase equilibria calculations (section 3) from the thermal evolution of the intrusion (section 4.1) because we are applying a new thermodynamic model (Weller et al., 2024), so it is beneficial to demonstrate how the system behaves in the simplest configuration (i.e. with imposed temperature increments), rather than the behaviour being coupled to assumptions regarding heat transfer with the surroundings, and/or mixing and circulation within the magma chamber. However, we also perform comparison calculations of energy-coupled assimilation by stoping and assimilation by partial country rock melting using the MCS (Bohrson et al., 2014), which has the additional role of comparing results using a different thermodynamic model (rhyolite-MELTS v.1.2.0; Gualda et al., 2012; Ghiorso and Gualda, 2015).

3. Results

3.1. Fractional crystallisation with no assimilation

The modelled compositional evolution of residual melts and mineral assemblages during fractional crystallisation are shown in Figs. 3a, 4 and S1, for varying fractionation pressure and xFe^{3+}. Model melt compositions (Fig. 3a) are compared to the reported whole-rock chemistry of YGDC rocks. At all considered pressures and xFe^{3+}, olivine is the first phase to crystallise, followed by spinel and plagioclase feldspar (Fig. 4). To lower temperatures, magnetite, clinopyroxene and ilmenite crystallise, with their relative order and abundance dependent on xFe^{3+}. Olivine and feldspar are volumetrically dominant during crystallisation.

The modelled melt remains silica-undersaturated across all considered crystallisation conditions without assimilation (Fig. 3a). Beyond 80% crystallisation the melt compositions curve upward in total alkali versus silica (TAS) space toward a variety of highly alkaline compositions. The specific evolution of melt composition varies with pressure or xFe^{3+} because these parameters affect the crystallising assemblage

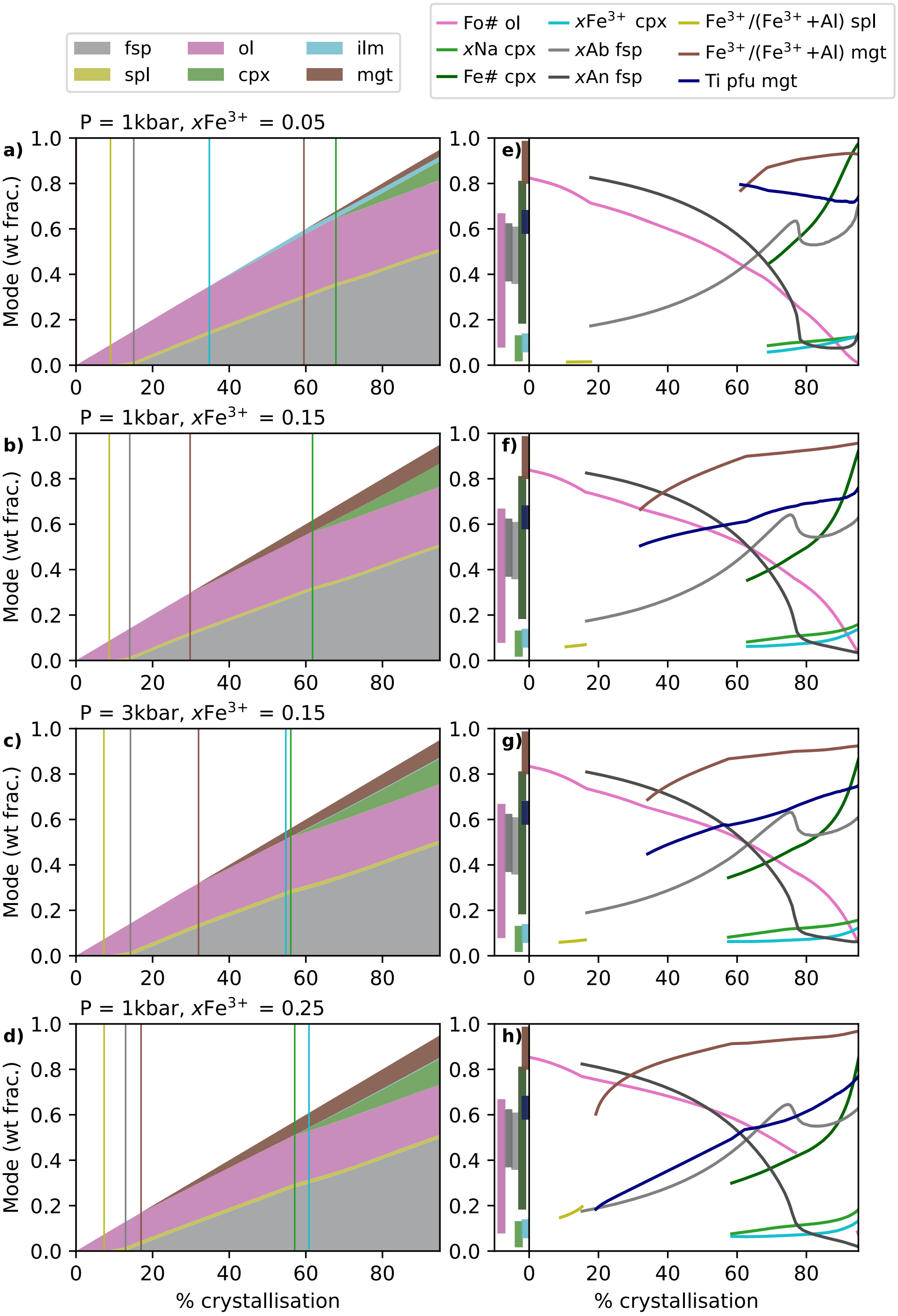

Fig. 4. Cumulative solid mineral assemblage (panels a–d) and mineral compositional evolution (panels e–h) during fractional crystallisation of primitive YGDC melt under varying pressure and $x\text{Fe}^{3+}$ conditions. Vertical lines in panels a–d highlight the appearance of mineral phases. % crystallisation defined as wt% of the initial intrusion mass remaining. Coloured bars in panels e–h show reported mineral compositional data from Upton and Thomas (1980); note that their position on the x-axis cannot be estimated because there is no corresponding reported whole-rock major element data for most of the samples.

(e.g. Fig. 4). For example, with increasing pressure for a given $x\text{Fe}^{3+}$, the melt evolution curves become increasingly silica-poor (Fig. 3a). This behaviour occurs because relatively silica-rich clinopyroxene appears earlier in the fractionation history and subsequently reaches higher cumulative modes during crystallisation at increasing pressure (green shading, Fig. 4c vs 4b), at the expense of olivine and anorthite-rich feldspar, which have lower silica content.

Increasing $x\text{Fe}^{3+}$ at a fixed pressure causes melt evolution curves to diverge early during fractionation and become increasingly separated in TAS space (Fig. 3a). This behaviour occurs because the earlier and more abundant crystallisation of magnetite at high $x\text{Fe}^{3+}$ (brown shading, Fig. 4d versus 4a, b) results in shallower initial melt evolution trajectories in TAS space. The divergence is exacerbated by earlier clinopyroxene crystallisation at higher $x\text{Fe}^{3+}$ combined with feldspar evolving from anorthite- to albite-rich compositions at about 75% crystallisation (Fig. 4).

In all cases, the model mineral assemblage is consistent with that reported for the YGDC of initial olivine and plagioclase-olivine cumulate rocks adjacent to the chilled margins, with more evolved exposed sequences containing varying minor (< 15 vol.%) clinopyroxene, ilmenite

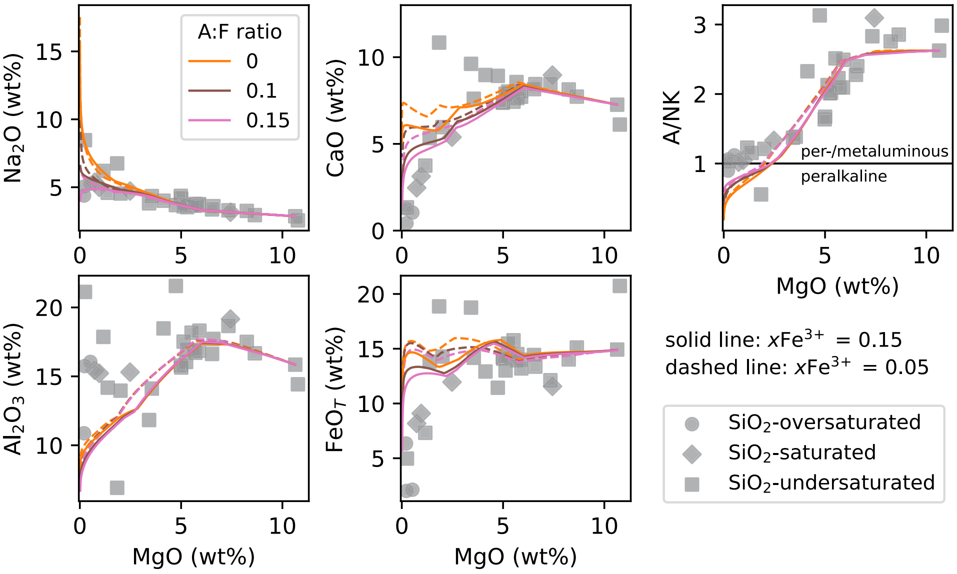

Fig. 5. Modelled major element evolution of melts during AFC of primitive YGDC. Results shown for 1 kbar calculations with A:F from 0–0.15, with xFe^{3+} = 0.05–0.15. Grey symbols are whole-rock compositions from the YGDC. A/NK = molar Al$_2$O$_3$/(Na$_2$O + K$_2$O).

and titanomagnetite (Upton and Thomas, 1980), also consistent with experimental studies on YGDC compositions (see Supplement). Mineral compositional trends observed in the YGDC are also reproduced by our models, such as calcic plagioclase in the chilled margins that becomes increasingly sodic with increasing degree of melt evolution, and reported olivine evolution to extremely fayalitic compositions (Fo$_4$; Upton and Thomas, 1980; Fig. 4).

The modelled evolved melt compositions for fractionation at 1 kbar with xFe^{3+} = 0.15–0.25, and crystallisation extent up to ~96%, match the reported YGDC whole-rock compositions of syenite to nepheline syenite (Fig. 3a). The modelled mineral compositions under the same conditions also match the reported range for feldspar, olivine, clinopyroxene and magnetite in the YGDC (Fig. 4). The effect of varying xFe^{3+} means that fractionation modelled at e.g. 2–3 kbar with initial xFe^{3+} = 0.25 will also produce nepheline syenite compositions (Fig. S1). However, this xFe^{3+} is higher than thought for the YGDC (Upton, 2013). Importantly, silica-oversaturated YGDC rocks as reported on Tuttutooq (Fig. 1, 3a, Upton, 2013) cannot be produced by fractional crystallisation from the primitive melts under any pressure or xFe^{3+} conditions studied here, implying that another process, such as crustal assimilation of more silica-rich compositions, is required.

3.2. Fractional crystallisation with assimilation

In this section we explore the compositional effects of assimilation with reference to two scenarios. First we consider simultaneous assimilation-fractional crystallisation (AFC). Second, we investigate single-stage assimilation followed by subsequent fractional crystallisation.

3.2.1. AFC

The key variable during AFC as formulated by DePaolo (1981) is the assimilation to fractionation ratio (A:F), a mass ratio of assimilated to fractionated material. The total mass of assimilated material during an AFC path is therefore a function of both fractionation extent and A:F. We show the modelled evolving melt compositions during AFC in TAS space in Fig. 3b for 1 kbar, with xFe^{3+} from 0.05–0.25 and A:F from 0.0–0.3, and fractional crystallisation to 98%. For figure clarity, not all A:F ratios are shown for all considered xFe^{3+}. The evolving melt chemistry in other major element oxides is shown in Fig. 5 for a subset of modelled A:F and xFe^{3+}, and additional results showing other modelled pressures and varying assimilant chemistry are provided in Figs. S2–3.

During modelled AFC scenarios with increasing A:F from to 0 to 0.3, the gradual addition of silica-rich crustal assimilant into the melt eventually results in silica-oversaturation. For plausible estimated YGDC crystallisation conditions of xFe^{3+} = 0.05–0.15 and up to ~2 kbar (Upton and Thomas, 1980; Upton, 2013), the range of reported YGDC compositions in TAS space can be matched by an A:F of $\lesssim 0.15$ (Fig. 3b for 1 kbar results; Fig. S2 for higher pressure). AFC evolution also reproduces the compositional range of the YGDC for other major elements (Fig. 5 for 1 kbar results), although we note a deviation to lower Al$_2$O$_3$ and higher CaO contents of model melts compared to some evolved YGDC rocks below ~ 5 wt% MgO. The high reported Al$_2$O$_3$ and CaO contents of some silica-undersaturated evolved rocks could only be generated by fractionation alone if anorthite-rich feldspar saturation was not reached, inconsistent with the reported petrography of these samples (Upton and Thomas, 1980), and may instead be reflecting feldspar accumulation not accounted for by our model. The modelled crystallising mineral assemblage during AFC with A:F up to 0.3 is very similar to that during fractional crystallisation models (Fig. 4), with an assemblage of olivine followed by spinel, plagioclase, Fe-Ti oxides and clinopyroxene, consistent with the observed YGDC petrography (section 3.1; Upton and Thomas, 1980). To test the sensitivity of our results to assimilant composition we performed the same calculations using an Archean gneiss (the host rock for intrusions north of the Tuttutooq region). The melt evolution results are similar to those for the Julianehåb granitoid, although to match the reported silica-oversaturated rock compositions, a lower A:F (~ 0.1) is required because the Archean gneiss has a lower alkali content (Fig. S3; Steenfelt et al., 2005).

Up to ~80% crystallisation, the residual melt compositions with increasing A:F plot in a similar region of TAS space for given crystallisation conditions. Importantly, however, they span the silica-saturation divide (Tuttle and Bowen, 1958), and therefore evolve beyond this point along compositionally divergent liquid lines of descent (Fig. 3b). To illustrate this divide we show a T–X pseudosection (Fig. 6a) for the 80% fractionated melts at 1 kbar and xFe^{3+} = 0.15, from A:F = 0 (X = 0) to A:F = 0.15 (X = 1). The solidus (bold line) features a concave downwards section about the maximum solidus temperature. This section is interpreted as a higher component expression of the plane of silica-oversaturation in the canonical quartz-nepheline-kalsilite system (Bowen, 1937), as leucite (red line) is a stable solidus phase at lower values of X and quartz (orange line) is stable at higher values (Fig. 6). These melts can therefore be classified according to their solidus assemblage (Fig. 6b), analogous to a normative mineralogy calculation,

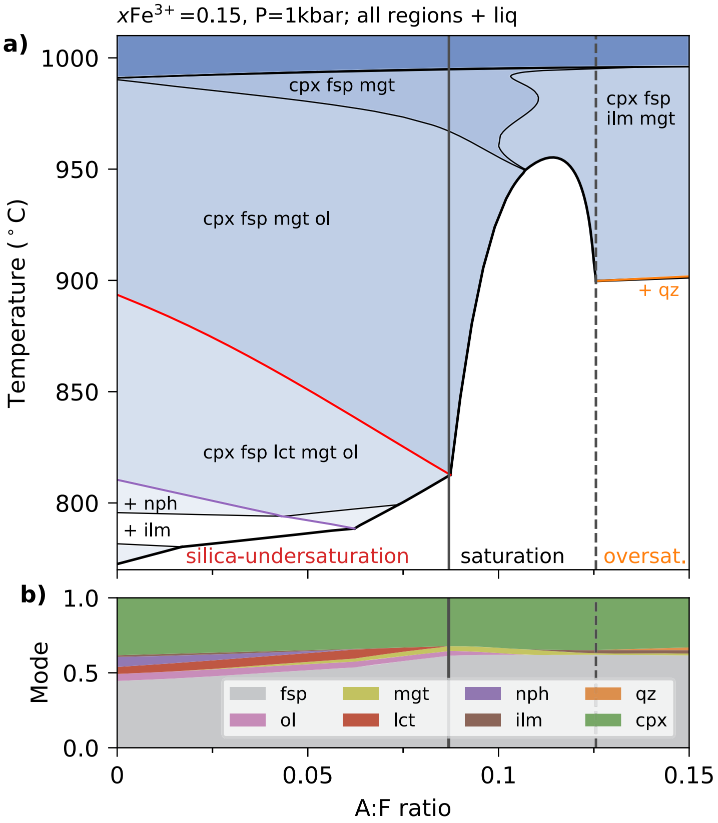

Fig. 6. (a) T–X pseudosection between melts generated at 80% crystallisation along AFC paths from Fig. 3b, for A:F = 0 ($X = 0$) to A:F = 0.15 ($X = 1$), at 1 kbar with initial $x\mathrm{Fe}^{3+} = 0.15$. This X vector crosses from silica-undersaturated (feldspathoid-bearing at their solidus), through silica-saturated (neither quartz or feldspathoid-bearing) to silica-oversaturated compositions (quartz-bearing). (b) Solidus mineralogy for (a). Abbreviations as per. Fig. 2, with the addition of nph = nepheline, qz = quartz.

as silica-undersaturated or silica-oversaturated respectively, with an intermediate region of silica-saturation (neither quartz nor feldspathoids present). For the model scenario in Fig. 6a where AFC stops at 80% fractionation and the residual melt undergoes in-situ batch crystallisation with no further assimilation (i.e. simulating incomplete AFC, where late residual melt fractions are unable to assimilate more material), an A:F of 0.13 results in silica-oversaturation. Such melts that have become silica-oversaturated would continue to evolve towards granitic compositions during crystallisation, even if no further assimilation occurred. While the exact numbers here are specific to the YGDC, this sharp transition between silica-undersaturated and silica-oversaturated melts in major element space will be generally applicable to silica-undersaturated melts undergoing assimilation.

3.2.2. Single-stage assimilation

Single-stage assimilation, where assimilant is added via stoping prior to any fractional crystallisation, provides a comparison to AFC. This calculation also allows us to explore the implication from Fig. 6 that melts cross a ‘tipping point’ in their evolution, beyond which they will evolve to silica-oversaturated granitic compositions without further assimilation.

Our results (Fig. S4b) show that $\lesssim$15% by mass addition of crustal assimilant is still required to generate the observed geochemical diversity in the YGDC, even when all assimilation is modelled as occurring prior to any fractional crystallisation. Sufficient addition of country rock granite into the initial basalt drives the bulk composition to no longer be silica-undersaturated, beyond which low pressure fractional crystallisation results in a silica-oversaturated final melt (Soderman et al., 2025).

3.2.3. Assimilation of partial country rock melts

The models above both consider assimilation via stoping, which we consider a reasonable simplification for the major element evolution of the case study region as partial melts of granitoids are similar to the whole-rock composition. However, another model of assimilation is through the partial melting of country rock, which is particularly important for trace element budgets (Heinonen et al., 2020, 2021a). In this case, assimilation will not start at the onset of fractional crystallisation because the country rock must first be heated by the crystallising magma. In Fig. S5 we show the major element results for two example modified AFC scenarios that begin to assimilate a partial melt of the Julianehåb granitoid after 50 and 70% crystallisation respectively (with A:F = 0.15, see Supplement for details). These example calculations highlight that stoping likely provides an upper limit to assimilated mass (e.g. ~7% by mass assimilation of granitic melt is required to match reported YGDC compositions if assimilation begins at 50% fractionation). This result is driven by (i) the country rock partial melt, although overall similar in major element composition, being slightly more silica-rich and alkali-poor than the bulk granite, and (ii) assimilation starting later during crystallisation.

4. Discussion

For plausible crystallisation conditions of the YGDC (~1–2 kbar, $x\mathrm{Fe}^{3+}$ of 0.05–0.15), $\leq$15% assimilated crust by mass is required to match reported whole-rock compositions in the YGDC and applies to a range of scenarios for assimilation and crystallisation. This result highlights that it may not always be possible to isolate the timing or style of assimilation by the evolved products of assimilation-crystallisation using a major element approach, albeit the approach is sensitive to mass fractions required. We consider the viability of this amount of assimilation using energy balance and isotopic constraints below, which can also be applied to other intrusions. Finally, we consider the general effects of pressure, oxidation state and bulk composition on melt evolution during assimilation-crystallisation that can be applied to alkaline complexes worldwide.

4.1. Energy balance limits to assimilated mass

An important constraint on the volume of material an igneous body can assimilate arises from the thermal energy balance of the intrusion. The assimilation of cooler country rock into a warmer igneous body will reduce the temperature of the intrusion (e.g. Nicholls and Stout, 1982; Sparks, 1986; Reiners et al., 1995; Thompson et al., 2002). If a sufficient volume of material is assimilated, the intrusion will therefore become too cool to assimilate any additional country rock. Added to this effect are the roles of the latent heat of crystallisation of the solidifying intrusion, and the rate of diffusive heat loss to the country rock. In this section we construct a simple thermal model considering these effects, and assess the thermally-viable levels of assimilation of country rock into the intrusion. To provide an indication of the relative importance of the effects we include, and to allow the results to be applied to a range of other intrusions, we describe the model in stages. We first only consider the effects of mixing country rocks into the melt, which assumes that crystal fractionation and heat transport to the wall rocks are negligible. That situation is relevant to cases where assimilation of country rocks into the magma is rapid compared to those other processes. We then include the effects of fractionation, in line with the AFC modelling described above. Finally, we also incorporate the effects of heat loss into the wall rocks.

We follow the approach of Thompson et al. (2002) in constructing a model that accounts for latent heat and the temperature effect of mixing country rock into the melt. Due to the uncertain rates of assimilation, fractionation, and magma transport, we do not undertake a fully-coupled physical and chemical magma chamber model (e.g. Bohrson et al., 2014; Heinonen et al., 2021b), and instead focus on exploring the effects of a small number of important free parameters. As detailed in the Supplement, we begin with melt and country rocks at a wide range of temperatures (spanning from supra-liquidus conditions to the approximate solidus for the melt/intrusion (T_i), and from 0–800 °C for the country-rock assimilant (T_a)). We calculate the mass of country rock, as a proportion of the mass of the intrusion (M_a/M_i), that can be assimilated before a temperature is reached at which further assimilation is no longer possible (T_{av}, which we take to be 900 °C – the solidus temperature of the silica-oversaturated evolved melt; Fig. 6). This calculation is the equivalent of the 'single-stage assimilation' model above: all viable assimilation happens immediately, before melt volume is lost through fractionation. Fig. 7a shows the result of such a calculation (using the right-hand labels on the colour scale). Two intuitively straightforward effects are visible: hotter intrusions can assimilate more country rock before becoming too cool to continue assimilating, and cooler country rocks have a larger effect on the intrusion temperature than warmer ones, and so reduce the amount of assimilation that is possible. For a likely intrusion temperature of 1000–1300 °C (the lower bound following Upton and Thomas (1980) that the absence of observed cumulate clinopyroxene from the primitive YGDC melts constrains a minimum intrusion temperature, and the upper bound taken as the liquidus temperature of the primitive YGDC, with both temperatures taken from Fig. 2 considering 1σ temperature uncertainties of ±50 °C) and country rock temperature of 100–200 °C (based upon the estimated ∼1–2 kbar intrusion depth; Upton and Thomas, 1980) the calculations imply that the melt could assimilate country rock equivalent to 50–100% of its mass.

Two important effects can be added to the above calculation, of relevance to some intrusions (including the YGDC). First, in the case of AFC, melt volume will be lost by fractionation whilst assimilation is occurring. Our estimated thermally-viable levels of assimilation will in that case apply to the last-crystallised melt, which survives until the solidus is reached. The mean amount of assimilation by the melt body as a whole will be half of that value, in the case that the rates of assimilation and fractionation are fully coupled, as in the AFC model (left-hand labels on the colour scale on Fig. 7a). Field and petrological inferences of limited migration and re-equilibration of intra-cumulate melt, and of complex convection currents in localised portions of the complex (Upton, 2013), mean that it is difficult to use available observations to constrain the degree of melt-assimilant contact, the rates of fractionation and assimilation, and the degree of chemical re-equilibration within the dyke. It is therefore not robustly known where on the spectrum between the two end-member cases considered here (represented by the left-hand and right-hand labels on the colour scale on Fig. 7a) is appropriate for the interior portions of the YGDC, but viable estimates for the maximum amount of possible assimilation range from those estimated above down to 25–50% country rock assimilation by mass.

The final effect that can be considered is diffusive heat loss to the surrounding country rocks, which is likely to be significant for a temperature difference across an intrusion margin on the order of 1000 °C (as is likely for the YGDC; see above). Such heat loss will reduce the amount of assimilation that is thermally viable, due to representing a reduction in the heat energy per mass within the dyke, additional to the effects of assimilation. We straightforwardly parameterise this effect as the percentage of the overall heat energy that is lost from the system. The effect on the viable amount of assimilation is shown on Fig. 7b for two model configurations that span the range of plausible values for the YGDC (i.e. the dashed region in Fig. 7a; see above), with the shaded areas showing the range of intermediate possible models for single-stage (red) and mean AFC (blue) assimilation models. To be consistent with the amount of assimilation suggested by the phase equilibria models described above (dotted line), the intrusion can lose no more than 10–30% of its heat before the required level of assimilation is not viable (with the value within that range depending on the intrusion and country rock temperatures, and the style of assimilation).

The characteristic thermal timescale for a variety of intrusion dimensions is shown in Fig. 7c. This timescale, calculated as $\tau = l^2/\pi^2\kappa$, where l is the intrusion dimension and κ is the thermal diffusivity, represents the time taken to reduce the temperature contrasts to a factor of $1/e$ of their original values, so will over-estimate the time taken to reduce the intrusion below 900 °C. However, these timescales are a useful guide for those above which assimilation cannot be significant. If the shortest dimension of the 'dyke' is the across-strike width (∼1 km), the relevant timescale is $\sim 10^3$ years. If the intrusion was assembled from smaller bodies with shorter lengthscales, then the corresponding timescale would be shorter (Fig. 7c). The map pattern of the lithological variations within the YGDC (Fig. 1b) and previous work on the southern branch of the intrusion (Koopmans et al., 2022) implies that the across-strike width is shorter than the lengthscale of any along-strike segmentation within the complex, so is likely to be the relevant lengthscale. For an intrusion of ∼1 km width (e.g. the region containing evolved rocks near Asorutit on Fig. 1) to assimilate 15% by mass of the country rock along the two lateral walls in a timescale of 10^3 years would require an outward propagation rate of each intrusion interface of 0.075 m/yr (assuming that across-strike growth is the dominant cause of assimilation, and assuming a constant ratio of mass to volume). These values are lower than those suggested in the literature for dissolution rates of solid rocks in melts (∼1–100 m/yr; McLeod and Sparks, 1998; Shaw, 2000) implying that either natural rates can be lower than previously estimated or, perhaps more likely, that the majority of assimilation in the YGDC happened rapidly, before the wall-rocks had become too shielded by crystallised material.

Taken together, the above arguments imply that it is thermally viable for the YGDC to assimilate a mass of country rock equivalent to the maximum proportion estimated by phase equilibrium modelling (∼ 15%) of its pre-fractionation volume, provided that assimilation is rapid compared to diffusive heat loss (in this case, occurring over shorter

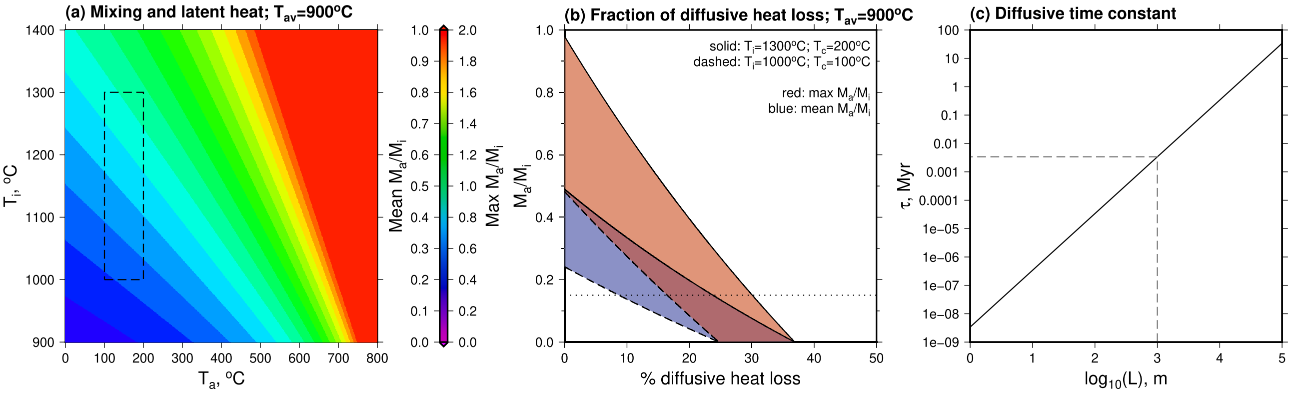

Fig. 7. Results of calculated energy balance limits on assimilation. (a) Mass of country rock that can be assimilated, per mass of intrusion (M_a/M_i), as a function of initial intrusion temperature (T_i), assimilation temperature (T_a), and assuming assimilation stops at 900 °C. The right-hand colour scale corresponds to single-step assimilation, and the left-hand to the mean value in an AFC model (see text for details). The black dashed rectangle highlights a conservatively-large range of plausible values for the YGDC. (b) M_a/M_i as a function of the percentage of heat energy in the intrusion that is lost from the system by diffusion. The black lines show single-step assimilation values for different values of T_i and T_a (labelled in top right), and the red area shows the range covered by models with intermediate values of these parameters. The blue shading is the equivalent values for the mean assimilation in an AFC model. The dotted line shows the mass ratio of assimilation (0.15) suggested by the geochemical arguments above. (c) The diffusive thermal time constant as a function of lengthscale, with the value relevant to the studied portion of the YGDC indicated.

timescales than 10^3 years), and provided that the intrusion temperature was sufficiently high. Reported along-strike variations in intrusion width and internal flow dynamics (Upton, 2013) will have resulted in along-strike variations in thermal timescales and the evolution of temperature within the intrusion. These effects could result in variations in the assimilated mass of country rock along-strike. Such effects may be one explanation for the observed geochemical variability between silica-undersaturated and -oversaturated evolved rocks along the length of the YGDC. Alternatively, variations along-strike in internal flow patterns and crystal-melt dynamics could have led to variability in the amount of contact between the melt and country rock, with a similar result.

4.1.1. *Consideration of coupled chemical and energy balance evolution*

Although we consider chemical and thermal behaviour separately to capture the important major element-based phase equilibria behaviour that is the focus of this work, energy-coupled scenarios can also provide important insights into assimilation behaviour (e.g. Spera and Bohrson, 2001; Bohrson et al., 2014). As a comparison to our results presented above, we model fractionation (Fig. S6) and assimilation via both stoping and wallrock melting (Fig. S7) using the energy-coupled Magma Chamber Simulator (MCS; Bohrson et al., 2014, see Supplement). The modelled melt compositions are not directly comparable to those presented above because they use a different underlying thermodynamic database, rhyolite-MELTS v.1.2.0 (Gualda et al., 2012). However, the results of the MCS calculations show similar melt compositional evolution trends as Fig. 3, with the examples shown producing silica-oversaturated granitic compositions at ∼20% assimilation by mass for stoping or ∼10% for country rock melting (Fig. S7). We note that the MCS results are non-unique as they require choices about a wide variety of physical and thermal parameters. However, these calculations provide a useful energy-coupled comparison, suggesting that our chemistry-only model reproduces the key major element behaviour of the system, and confirms the thermal viability of such assimilant masses.

4.2. *Isotopic constraints*

Radiogenic isotope systematics (e.g. Sr and Nd isotopes) across the wider rift system in southern Greenland indicate a role for crustal assimilation in many of the intrusions (Taylor and Upton, 1993; Goodenough, 1997; Stevenson et al., 1997; Goodenough et al., 2002; Upton et al., 2003). For the YGDC, published isotope data are limited (especially for Sr), but cover a range of $^{87}Sr/^{86}Sr_i \approx 0.703$–$0.704$ when samples flagged as altered are removed (Goodenough, 1997) and $\epsilon Nd_i \approx -3$ to $+1$ (± approx. 0.5, Goodenough, 1997; Beard et al., 2024; i denotes values corrected to the YGDC emplacement age). To estimate the isotopic signal of adding country rock into the primitive YGDC, we perform three calculations for different assimilation scenarios: 1) the single-stage addition of crustal material (i.e. binary mixing), 2) AFC following DePaolo (1981), where assimilation occurs via stoping as in Fig. 3, and 3) energy-coupled AFC using the MCS where assimilation of partial country rock melts occurs. The parameters used for these calculations are given in Tables S4–6, and relevant equations given in the Supplement.

These calculations show that the addition of 15% by mass of Julianehåb granite into the primitive YGDC would cause ϵNd and $^{87}Sr/^{86}Sr$ to vary by ∼−2.5 and +0.0009 respectively for single-stage addition, ∼−3 and +0.014 for AFC through stoping (A:F = 0.15), and ∼−6 and +0.004 for AFC through partial melting (Fig. S8). The larger impact on $^{87}Sr/^{86}Sr$ during AFC via stoping than single-stage assimilation occurs because of the compatibility of Sr in the fractionating feldspar, which consequently reduces Sr concentration in the late stage AFC residual melts and results in assimilant having a larger effect on melt $^{87}Sr/^{86}Sr$. Conversely, the smaller variation in $^{87}Sr/^{86}Sr$ during AFC via country rock melting compared to stoping occurs because of the compatibility of Sr in the feldspar-rich residual country rock, such that relatively little Sr is added into the fractionating magma (Heinonen et al., 2020). Such differences in isotopic behaviour between assimilation scenarios means that an isotopic study could allow for the identification of single-stage assimilation or different AFC mechanisms, which cannot easily be distinguished from major element geochemistry (Heinonen et al., 2020).

In the YGDC, only four samples have reported $^{87}Sr/^{86}Sr$ and ϵNd data that are not identified as potentially altered (Goodenough, 1997; Upton et al., 2003). Although the data are limited, their scatter towards lower ϵNd than the proposed primitive melt supports assimilation (Fig. S8), but a particular assimilation scenario cannot yet be identified, and the measured samples do not include the evolved rocks that would show maximum isotopic variation.

The reported trace element composition and isotope compositions of the country rock are variable, and using alternative compositional data for the Julianehåb granite (e.g. from Halama et al., 2003 rather than Stevenson et al., 1997; Table S3), the same range of Sr and Nd isotope compositions in the intrusion as produced in the 15% single-stage assimilation calculation above would be generated by <10% single-stage assimilation for ϵNd, and >20% single-stage assimilation for $^{87}Sr/^{86}Sr$. Such uncertainty and/or variation in assimilant trace element chemistry may contribute to both large and wide-ranging estimates of assimilation masses in alkaline-silicate complexes, both in south Greenland in Ilim-

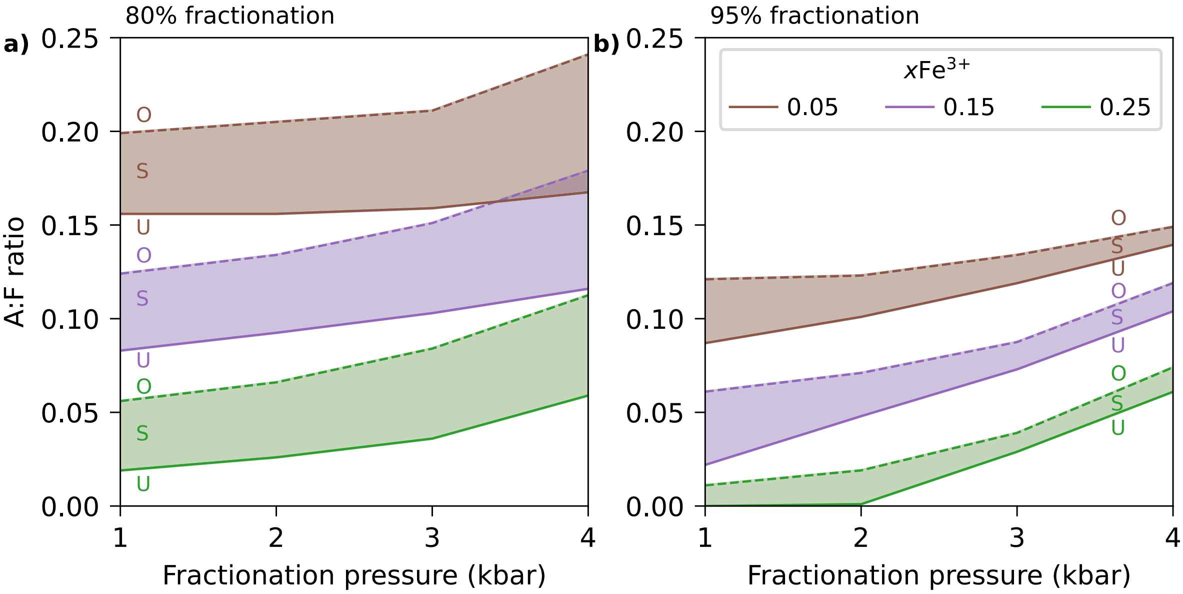

Fig. 8. The impact of varying pressure and xFe^{3+} on the A:F ratio required to reach silica-undersaturated (U), -saturated (S) or -oversaturated (O) residual melts, at 80% (a) and 95% fractionation (b).

maasaq (e.g. Stevenson et al., 1997) and worldwide (e.g. Landoll and Foland, 1996; Martinez et al., 1996; Ódri et al., 2020). Consequently, isotope data may not always be as successful at tightly constraining amounts of crustal assimilation as a phase equilibria approach, especially where the isotopic characterisation of the assimilant is highly variable or poorly known (e.g. Landoll and Foland, 1996) in comparison to its major element chemistry. However, an isotopic approach (if the melt and assimilant compositions are well-constrained) may provide greater insight into the style of assimilation than the major element chemistry.

4.3. Global implications: effects of pressure, fO_2 and bulk composition

Due to the impact of xFe^{3+} and pressure on the alkali and silica enrichment in the residual melt during fractionation (Fig. 3a), both parameters will affect the rate of crustal assimilation needed to achieve a transition from evolved silica-undersaturated to -oversaturated melts. We explore the effect of these parameters using a ‘regime’ diagram constructed for the results of AFC models (via stoping) to 80 and 95% crystallisation (Fig. 8). In each case, for the considered pressure (x-axis) and xFe^{3+} (different colours), AFC is stopped at the given point of fractionation, with the solid lines showing the transition in the residual melts from silica-undersaturation (U) to -saturation (S), and dashed lines from -saturation to -oversaturation (O). Overall, the results show that decreasing pressure or increasing xFe^{3+} (from brown to purple to green shading) reduces the required A:F to achieve silica-oversaturated residual melts, due mainly to the pressure-dependent behaviour of clinopyroxene and magnetite crystallisation as outlined in section 3.1. Lower A:F ratios are also needed if assimilation is stopped later in the crystallisation history (Fig. 8a versus 8b); an expected behaviour because assimilation occurs as a mass proportion of fractionation during AFC. Comparing the results at 80 and 95% fractionation also reveals that the silica-saturation window (i.e. the intervals between the solid and dashed lines; see also Fig. 6) narrows as fractionation increases, which we interpret as a higher component expression of the silica-undersaturation and -oversaturation planes of the basalt tetrahedron (Yoder Jr. and Tilley, 1962) converging in the evolved quartz-nepheline-kalsilite system (Tuttle and Bowen, 1958).

Collectively, these results suggest that lower pressures, more oxidised conditions, and greater extents of fractionation lead to lower required assimilant mass to achieve silica-oversaturation from a silica-undersaturated primitive melt. Such behaviour may be another explanation for the along-strike variability of the evolved compositions within the YGDC, where although up to 15% assimilation produces the observed silica-oversaturated compositions, a small decrease in magma fO_2 would lead to the same amount of assimilation producing silica-saturated to undersaturated assemblages. Changes in fractionation pressure along the length of the intrusion could also contribute to some variation in silica-saturation state from the same amount of assimilation. Although the YGDC provides an excellent natural laboratory in which to test these ideas, the concepts are more generally applicable where assimilation is thought to be relevant because the compositional evolution of melts to stronger silica-undersaturation with increasing pressure or decreasing xFe^{3+} is seen for other basaltic compositions (e.g. a global average silica-undersaturated trachybasalt from Cox, 1971, Fig. S9), as the same mineralogical effects control melt evolution with pressure or xFe^{3+}.

While the model system used here is anhydrous, we note that small amounts of water have been shown to slightly suppress alkali enrichment in fractionating primitive melts close to the silica-undersaturation/-saturation divide (Soderman et al., 2025), an effect supported by our comparison results performed in the MCS (Fig. S6). The implication is that drier silica-undersaturated magmas may require more assimilation to become silica-oversaturated than more hydrous magmas, although further investigation of this process will require calibration of a hydrous alkaline melt model.

Melt silica-saturation state has important implications for the type, size and mineralogy (and therefore economic viability) of critical metal deposits that can be found in alkaline-silicate complexes (Beard et al., 2023), such as the Ilimmaasaq complex thought to be ultimately derived from the same parental melt as the YGDC (Upton, 2013). For example, the unwanted early saturation of accessory rare earth element and high field strength element minerals may be delayed in highly alkaline silica-undersaturated melts (Beard et al., 2023), whereas sufficient assimilation of silicic country rocks may locally and abruptly decrease a melt’s metal-carrying capacity (Finch et al., 2019; Beard et al., 2023), terminating magmatic enrichment. Our results therefore imply that both primitive silica-undersaturated melts crystallising at higher pressures and those that are more reduced (and potentially driest) are most ‘resistant’ to becoming silica-oversaturated via crustal contamination, favouring the formation of large silica-undersaturated intrusions and impacting their subsequent mineralisation potential. This suggestion is consistent with differentiation at low fO_2 (and low water activity) being a characteristic feature of the most agpaitic (strongly peralkaline) alkaline-silicate rocks, and the world's largest silica-undersaturated intrusions (e.g. Ilimmaasaq, Lovozero and Khibiny, Pilanesberg; Marks and Markl, 2017).

5. Conclusion

Using a case study of the laterally-extensive Younger Giant Dyke Complex in south Greenland, which variably crystallised inwards to evolved silica-undersaturated and -oversaturated compositions along strike, we use thermodynamic models to quantify the effects of assimilation of country rock granite on the compositional evolution of a primitive silica-undersaturated basaltic melt during crystallisation. Small amounts of assimilated material (e.g. $\leq 15\%$ by mass for this case study) drive residual melts across the silica-undersaturation to -oversaturation divide and result in a variety of evolved rock compositions from nepheline syenites to granites. Although thermal and isotopic modelling are complementary approaches to the quantification of crustal assimilation, providing consistent results, our phase equilibria approach can more tightly constrain amounts of assimilant because the boundary between the two crystallisation regimes (to granite versus nepheline syenite) occurs over a narrow compositional range, and because relevant isotopic and thermal model parameters are typically less well constrained. Our results provide a globally relevant framework for predicting the range of petrogenetic conditions that favour a silica-undersaturated melt remaining highly alkaline during ascent and crystallisation, with more assimilation required to generate silica-oversaturated compositions when fractionating silica-undersaturated melts at higher pressures and/or more reduced conditions. The identification of such conditions may be an important part of understanding the processes by which some alkaline-silicate complexes develop evolved components with large critical metal deposits and others do not.

CRediT authorship contribution statement

Caroline R. Soderman: Writing – review & editing, Writing – original draft, Methodology, Investigation, Conceptualization. **Owen M. Weller:** Writing – review & editing, Writing – original draft, Investigation, Funding acquisition, Conceptualization. **Alex Copley:** Writing – review & editing, Writing – original draft, Methodology, Investigation. **Adrian A. Finch:** Writing – review & editing, Conceptualization. **Charles D. Beard:** Writing – review & editing.

Declaration of competing interest

The authors declare that they have no known competing financial interests or personal relationships that could have appeared to influence the work reported in this paper.

Acknowledgements

CRS and OMW were supported by a UKRI FLF [grant MR/V02292X/1]. AC was partly supported by NERC grant NE/W00562X/1. CB was supported by the Netherlands sectorplan scheme for scientific research and university education.

Appendix A. Supplementary material

Supplementary material related to this article can be found online at https://doi.org/10.1016/j.epsl.2025.119516.

Data availability

No data was used for the research described in the article.

References

Beard, C.D., Goodenough, K.M., Borst, A.M., Wall, F., Siegfried, P.R., Deady, E.A., Pohl, C., Hutchison, W., Finch, A.A., Walter, B.F., et al., 2023. Alkaline-silicate REE-HFSE systems. Econ. Geol. 118 (1), 177–208.

Beard, C.D., Finch, A.A., Borst, A.M., Goodenough, K.M., Hutchison, W., Millar, I.L., Andersen, T., Williams, H.M., Weller, O.M., 2024. A phlogopite-bearing lithospheric mantle source for Europe's largest REE-HFSE belt: Gardar Rift, SW Greenland. Earth Planet. Sci. Lett. 640, 118780.

Bohrson, W.A., Spera, F.J., 2001. Energy-constrained open-system magmatic processes ii: application of energy-constrained assimilation–fractional crystallization (ec-afc) model to magmatic systems. J. Petrol. 42 (5), 1019–1041.

Bohrson, W.A., Spera, F.J., Ghiorso, M.S., Brown, G.A., Creamer, J.B., Mayfield, A., 2014. Thermodynamic model for energy-constrained open-system evolution of crustal magma bodies undergoing simultaneous recharge, assimilation and crystallization: the magma chamber simulator. J. Petrol. 55 (9), 1685–1717.

Bohrson, W.A., Spera, F.J., Heinonen, J.S., Brown, G.A., Scruggs, M.A., Adams, J.V., Takach, M.K., Zeff, G., Suikkanen, E., 2020. Diagnosing open-system magmatic processes using the magma chamber simulator (mcs): part I—major elements and phase equilibria. Contrib. Mineral. Petrol. 175, 1–29.

Bowen, N.L., 1937. Recent high-temperature research on silicates and its significance in igneous geology. Am. J. Sci. 5 (193), 1–21.

Brandeis, G., Jaupart, C., 1987. The kinetics of nucleation and crystal growth and scaling laws for magmatic crystallization. Contrib. Mineral. Petrol. 96, 24–34.

Chen, J., Henderson, C.M.B., Foland, K.A., 1994. Open-system, sub-volcanic magmatic evolution: constraints on the petrogenesis of the Mount Brome alkaline complex, Canada. J. Petrol. 35 (4), 1127–1153.

Cox, K., 1971. Understanding the Earth - chapter 1: Minerals and Rocks. MIT Press. ISBN 0632036567 9780632036561.

DePaolo, D.J., 1981. Trace element and isotopic effects of combined wallrock assimilation and fractional crystallization. Earth Planet. Sci. Lett. 53 (2), 189–202.

Finch, A.A., McCreath, J.A., Reekie, C.D.J., Hutchison, W., Ismaila, A., Armour-Brown, A., Andersen, T., Simonsen, S.L., 2019. From mantle to Motzfeldt: a genetic model for syenite-hosted Ta, Nb-mineralisation. Ore Geol. Rev. 107, 402–416.

Foland, K.A., Landoll, J.D., Henderson, C.M.B., Chen, J., 1993. Formation of cogenetic quartz and nepheline syenites. Geochim. Cosmochim. Acta 57 (3), 697–704.

Ghiorso, M.S., Gualda, G.A., 2015. An h_2o–co_2 mixed fluid saturation model compatible with rhyolite-melts. Contrib. Mineral. Petrol. 169, 1–30.

Goodenough, K.M., 1997. Geochemistry of Gardar intrusions in the Ivigtut area, South Greenland. PhD thesis. University of Edinburgh.

Goodenough, K.M., Upton, B.G.J., Ellam, R.M., 2002. Long-term memory of subduction processes in the lithospheric mantle: evidence from the geochemistry of basic dykes in the Gardar province of south Greenland. J. Geol. Soc. 159 (6), 705–714.

Green, E.C., Holland, T.J., Powell, R., Weller, O.M., Riel, N., 2025. Corrigendum to: melting of peridotites through to granites: a simple thermodynamic model in the system kncfmashtocr, and, a thermodynamic model for the subsolidus evolution and melting of peridotite. J. Petrol. 66 (1), egae079.

Gualda, G.A., Ghiorso, M.S., Lemons, R.V., Carley, T.L., 2012. Rhyolite-melts: a modified calibration of melts optimized for silica-rich, fluid-bearing magmatic systems. J. Petrol. 53 (5), 875–890.

Halama, R., Wenzel, T., Upton, B.G.J., Siebel, W., Markl, G., 2003. A geochemical and Sr-Nd-O isotopic study of the proterozoic Eriksfjord Basalts, Gardar province, south Greenland: reconstruction of an OIB signature in crustally contaminated rift-related basalts. Mineral. Mag. 67 (5), 831–853.

Harris, C., Marsh, J.S., Milner, S.C., 1999. Petrology of the alkaline core of the Messum igneous complex, Namibia: evidence for the progressively decreasing effect of crustal contamination. J. Petrol. 40 (9), 1377–1397.

Heinonen, J.S., Bohrson, W.A., Spera, F.J., Brown, G.A., Scruggs, M.A., Adams, J.V., 2020. Diagnosing open-system magmatic processes using the magma chamber simulator (mcs): part ii—trace elements and isotopes. Contrib. Mineral. Petrol. 175, 1–21.

Heinonen, J.S., Iles, K.A., Heinonen, A., Fred, R., Virtanen, V.J., Bohrson, W.A., Spera, F.J., 2021a. From binary mixing to magma chamber simulator: geochemical modeling of assimilation in magmatic systems. In: Crustal Magmatic System Evolution: Anatomy, Architecture, and Physico-Chemical Processes, pp. 151–176.

Heinonen, J.S., Spera, F.J., Bohrson, W.A., 2021b. Thermodynamic limits for assimilation of silicate crust in primitive magmas. Geology 50, 81–85. https://doi.org/10.1130/G49139.1.

Holland, T.J.B., Powell, R., 2011. An improved and extended internally consistent thermodynamic dataset for phases of petrological interest, involving a new equation of state for solids. J. Metamorph. Geol. 29 (3), 333–383.

Kalsbeek, F., Taylor, P.N., 1985. Isotopic and chemical variation in granites across a proterozoic continental margin—the Ketilidian mobile belt of south Greenland. Earth Planet. Sci. Lett. 73 (1), 65–80.

Köhler, J., Schönenberger, J., Upton, B., Markl, G., 2009. Halogen and trace-element chemistry in the Gardar province, south Greenland: subduction-related mantle metasomatism and fluid exsolution from alkalic melts. Lithos 113 (3–4), 731–747.

Koopmans, L., McCarthy, W., Magee, C., 2022. Dyke architecture, mineral layering, and magmatic convection; new perspectives from the Younger Giant Dyke complex, S Greenland. Geochem. Geophys. Geosyst. 23 (3), e2021GC010260.

Landoll, J.D., Foland, K.A., 1996. The formation of quartz syenite by crustal contamination at Mont Shefford and other monteregian complexes, Quebec. Can. Mineral. 34, 301–324.

Marks, M.A.W., Markl, G., 2015. The Ilímaussaq Alkaline Complex, South. Greenland. Springer, pp. 649–691.

Marks, M.A.W., Markl, G., 2017. A global review on agpaitic rocks. Earth-Sci. Rev. 173, 229–258.

Martinez, I.A., Harris, C., Le Roex, A.P., Milner, S.C., 1996. Oxygen isotope evidence for extensive crustal contamination in the Okenyenya igneous complex, Namibia. Geochim. Cosmochim. Acta 60 (22), 4497–4508.

McLeod, P., Sparks, R., 1998. The dynamics of xenolith assimilation. Contrib. Mineral. Petrol. 132, 21–33. https://doi.org/10.1007/s004100050402.

Möller, V., Williams-Jones, A.E., 2016. Petrogenesis of the Nechalacho layered suite, Canada: magmatic evolution of a REE–Nb-rich nepheline syenite intrusion. J. Petrol. 57 (2), 229–276.

Neumann, E.-R., 1980. Petrogenesis of the Oslo region larvikites and associated rocks. J. Petrol. 21 (3), 499–531.

Nicholls, J., Stout, M., 1982. Heat effects of assimilation, crystallization, and vesiculation in magmas. Contrib. Mineral. Petrol. 81, 328–339. https://doi.org/10.1007/BF00371687.

Ódri, Á., Harris, C., Le Roux, P., 2020. The role of crustal contamination in the petrogenesis of nepheline syenite to granite magmas in the Ditrău complex, Romania: evidence from O-, Nd-, Sr- and Pb-isotopes. Contrib. Mineral. Petrol. 175, 1–25.

Rämö, O.T., Andersen, T., Whitehouse, M.J., 2022. Timing and petrogenesis of the permo-carboniferous larvik plutonic complex, Oslo rift, Norway: new insights from U–Pb, Lu-Hf, and o isotopes in zircon. J. Petrol. 63 (12), egac116.

Reiners, P., Nelson, B., Ghiorso, M., 1995. Assimilation of felsic crust by basaltic magma: thermal limits and extents of crustal contamination of mantle-derived magmas. Geology 23, 563–566. https://doi.org/10.1130/0091-7613(1995)023<0563:AOFCBB>2.3.CO;2.

Riel, N., Kaus, B.J.P., Green, E.C.R., Berlie, N., 2022. MAGEMin, an efficient Gibbs energy minimizer: application to igneous systems. Geochem. Geophys. Geosyst. 23 (7), e2022GC010427.

Riishuus, M.S., Peate, D.W., Tegner, C., Wilson, J.R., Brooks, C.K., Harris, C., 2006. Temporal evolution of a long-lived syenitic centre: the Kangerlussuaq alkaline complex, East Greenland. Lithos 92 (1–2), 276–299.

Roulleau, E., Stevenson, R., 2013. Geochemical and isotopic (Nd–Sr–Hf–Pb) evidence for a lithospheric mantle source in the formation of the alkaline Monteregian province (Quebec). Can. J. Earth Sci. 50 (6), 650–666.

Shaw, C., 2000. The effect of experiment geometry on the mechanism and rate of dissolution of quartz in basanite at 0.5 GPa and 1350 C. Contrib. Mineral. Petrol. 139, 509–525. https://doi.org/10.1007/s004100000153.

Soderman, C.R., Weller, O.M., Beard, C.D., Riel, N., Green, E.C.R., Holland, T.J.B., 2025. A mid-crustal tipping point between silica-undersaturated and silica-oversaturated magmas. Nat. Geosci., 1–8.

Sparks, R.S.J., 1986. The role of crustal contamination in magma evolution through geological time. Earth Planet. Sci. Lett. 78, 211–223. https://doi.org/10.1016/0012-821X(86)90062-2.

Spera, F.J., Bohrson, W.A., 2001. Energy-constrained open-system magmatic processes I: general model and energy-constrained assimilation and fractional crystallization (ec-afc) formulation. J. Petrol. 42 (5), 999–1018.

Steenfelt, A., Garde, A.A., Moyen, J.-F., 2005. Mantle wedge involvement in the petrogenesis of archaean grey gneisses in West Greenland. Lithos 79 (1–2), 207–228.

Stevenson, R., Upton, B.G.J., Steenfelt, A., 1997. Crust-mantle interaction in the evolution of the Ilímaussaq complex, south Greenland: Nd isotopic studies. Lithos 40 (2–4), 189–202.

Taylor, P.N., Upton, B.G.J., 1993. Contrasting Pb isotopic compositions in two intrusive complexes of the Gardar Magmatic province of south Greenland. Chem. Geol. 104 (1–4), 261–268.

Thompson, A.B., Matile, L., Ulmer, P., 2002. Some thermal constraints on crustal assimilation during fractionation of hydrous, mantle-derived magmas with examples from central Alpine batholiths. J. Petrol. 43, 403–422. https://doi.org/10.1093/petrology/43.3.403.

Tuttle, O.F., Bowen, N.L., 1958. Origin of Granite in the Light of Experimental Studies in the System NaAlSi3O8–KAlSi3O8–SiO2–H2O. GSA Memoirs, vol. 57.

Upton, B.G.J., 1987. Gabbroic, syenogabbroic and syenitic cumulates of the Tugtutoq younger Giant Dyke complex, south Greenland. In: Origins of Igneous Layering. Springer, pp. 93–123.

Upton, B.G.J., 2013. Tectono-magmatic evolution of the younger gardar southern rift, south Greenland. GEUS Bull. 29 (1).

Upton, B.G.J., Fitton, J.G., 1985. Gardar dykes North of the igaliko syenite complex, southern Greenland. Rapp. Grønl. Geol. Unders. 127, 1–24.

Upton, B.G.J., Thomas, J.E., 1980. The tugtutoq younger giant dyke complex, south Greenland: fractional crystallization of transitional olivine basalt magma. J. Petrol. 21 (1), 167–198.

Upton, B.G.J., Stephenson, D., Martin, A.R., 1985. The tugtutôq older giant dyke complex: mineralogy and geochemistry of an alkali gabbro-augite-syenite-foyaite association in the gardar province of south Greenland. Mineral. Mag. 49 (354), 623–642.

Upton, B.G.J., Emeleus, C.H., Heaman, L.M., Goodenough, K.M., Finch, A.A., 2003. Magmatism of the mid-proterozoic Gardar province, south Greenland: chronology, petrogenesis and geological setting. Lithos 68 (1–2), 43–65.

Weller, O.M., Holland, T.J.B., Soderman, C.R., Green, E.C.R., Powell, R., Beard, C.D., Riel, N., 2024. New thermodynamic models for anhydrous alkaline-silicate magmatic systems. J. Petrol., egae098.

Yoder Jr., H.S., Tilley, C.E., 1962. Origin of basalt magmas: an experimental study of natural and synthetic rock systems. J. Petrol. 3 (3), 342–532.